Universiteit
Leiden
The Netherlands

Dislocations in stripes and lattice Dirac fermions

Mesaroš, A.

Citation
Mesaroš, A. (2010, October 6). *Dislocations in stripes and lattice Dirac fermions*. *Casimir PhD Series*. Retrieved from https://hdl.handle.net/1887/16013

Version:	Corrected Publisher's Version
License:	Licence agreement concerning inclusion of doctoral thesis in the Institutional Repository of the University of Leiden
Downloaded from:	https://hdl.handle.net/1887/16013

Note: To cite this publication please use the final published version (if applicable).

Chapter 4

Electronic States of Graphene Grain Boundaries

4.1 Introduction

Grain boundaries and other extended defect structures in graphite have been observed and studied by surface measuring techniques for a long time [166–169]. Such research actually reaches beyond the fundamental questions of mechanical material properties and crystalline ordering complexities: The properties of the surface (top) layer of defected graphite must be similar to the properties of an isolated graphene sheet with defects. In this context grain boundaries have a special status, in that they are extended along a line in the two-dimensional graphene, and they also carry a topological charge: In terms of the lattice order they can be represented as an array of dislocations with Burgers vectors that are aligned. [170] The subject of this Chapter is therefore closely tied to the themes of Chapters 2, 3. The focus on surface microscopic measurements however brings in the microscopic structure of the defect cores, and we will therefore encounter much new content.

The STS studies of graphite have also revealed some clues about the connection of extended defects and the controversial ferromagnetic properties of metal-free carbon. [171] Theoretical studies, aimed primarily at localized defects in graphene, [172, 173] also give insight into the electronic states and magnetic properties of some types of graphene edges, cracks, and single atom defects. However, basic studies of the extended defect structures themselves have been completely absent until recently. [170]

The recent STM and STS studies of the electronic properties [171, 174] have shown that the local density of states (LDOS) has two types of characteristic features: an enhancement at zero energy, or two peaks below and above zero energy. A first-principles model of grain boundaries based on periodic array of the simplest pentagon-heptagon dislocations [170] revealed the possibility of forming bands around zero energy when the dislocations are close to each other, accounting for the LDOS peaks at finite energies.

The aim of this Chapter is to further the theoretical knowledge about extended defect structures by analyzing the electronic structure of amorphous tilt grain boundaries in graphene, expecting the results to be directly applicable to measurements on the surface of graphite. Our approach is based on considering the relaxed boundary of misaligned grains of graphene, and the results should be of direct relevance to the structures found along the grain boundaries as seen on the surface of graphite. [175] We find that the disordered structures formed at the relaxed boundary between two differently oriented grains can have enhanced LDOS at zero, or at finite energies. These features result from narrow bands (localized states) that can form both near and away from zero energy.

We also discuss using simple dislocation arrays as grain boundary models, focusing on the fact that the dislocation core need not be the simplest pentagon-heptagon structure. [176] This can lead to LDOS enhancement at zero energy as seen in the STM measurements, but not available within the model of Ref. [170]. Finally, we also find a limit in which the low energy continuum theory of dislocated graphene precisely agrees with the tight-binding model results. Very intriguingly, such a theory predicts the appearance of localized zero energy states in an array of well separated dislocations, although this has not been observed in the first principles calculations of Ref. [170].

4.2 Dislocations in graphene as base of grain boundary models

Dislocation models of grain boundaries rely on the fact that an array of dislocations with same Burgers vectors produces a boundary line between two crystal domains of different lattice orientations [177–179]. In this Section we make observations relevant to such models in graphene.

4.2.1 Graphene dislocation structure in tight-binding

Simple dislocation cores in graphene come in two shapes that we label “PH core” and “OCT core” (cf. Fig. 4.1(a),(b)), both of which were shown to be stable lattice configurations. [176, 180] Geometrically, the two possibilities arise because the Bravais lattice has two atoms (separated by $\mathbf{\Delta}$) in the unit-cell, so that there are two inequivalent mutual configurations of $\mathbf{\Delta}$ and the Burgers vector $\vec{b}$. The LDOS at the atoms forming the core has been considered, [176, 181]

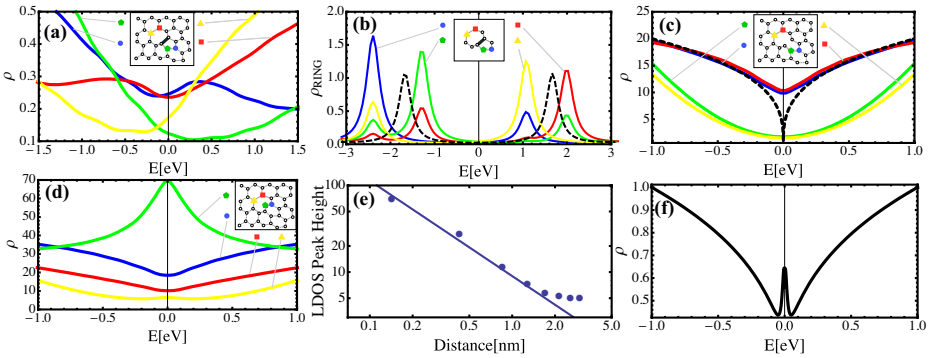

Figure 4.1: The LDOS of graphene dislocations from tight-binding and continuum theory. (a) LDOS of representative atoms of the "PH" type dislocation core (inset, see Section 4.2.1). The weight is shifted due to AA bond (thick in inset), compared to curves in (c). (b) The influence of AA bond on an isolated ring. (c) "PH" core LDOS without the AA bond. Dislocation topology effects from continuum theory (Section 4.2.2, dashed black curve) are prominent. (Finite LDOS at $E = 0$ is a finite size effect.) (d) LDOS of representative atoms in "OCT" core type. (e) The height of LDOS peak in (d) (pentagon, green) falls of like a power-law with distance from defect core. This holds also for LDOS features in (a). (f) The continuum defect topology prediction of LDOS (in patch of radius $\delta = 0.1$, Section 4.2.2) in a dislocation array, with zero modes.

revealing a sharp peak at zero energy in case of the "OCT" core, due to the undercoordinated atom. Note that even if only $\pi-$orbitals are considered, the single excess atom in one sublattice is responsible for the LDOS peak and the accompanying unbalanced magnetic moment in the presence of interactions. [176, 182–184] Alternatively, the "OCT" core can be viewed as a piece of a zigzag graphene edge of minimal length of one atom embedded in the graphene bulk, leading to same conclusions about its LDOS features. [172, 185–190]

Ref. [170] considers only "PH" type cores as building blocks of grain boundaries, and such models have been proposed in earlier graphite STM measurements. [166,191] However, the zigzag oriented grain boundary model of Ref. [171], as well as simple geometrical considerations we present above, both show that the arrays of "OCT" type dislocations should not be disregarded in real materials, even if they are more energetically costly than the "PH" type.

The inclusion of the "OCT" dislocations can be important for explaining the observed LDOS peaks at zero energy in the measurements of Ref. [171]. The set of grain boundaries considered there shows that such LDOS features are found only when the defect cores are well separated (i.e. the grain boundary angle is small). One might assume that when the defects are closer to each other, the zero energy states hybridize and move to finite energies. We have however found that

the localized zero energy modes are robust even when the defects are brought next to each other, which would be the case in a grain boundary with maximal opening angle.

Our analysis was done by considering the LDOS of defects set inside a 75x75 unit-cell sized graphene patch tight-binding model, with twisted periodic boundary conditions in both directions. The special boundary conditions enable the system under consideration to actually be a periodic, 10x10 sized arrangement with the graphene patches as unit-cells, thereby leading to a tenfold increase in linear system size and a correspondingly denser energy spectrum E_n (with corresponding eigenfunctions ψ_n), from which the LDOS $\rho(i, E)$ at site i and energy E follows in a standard way:

$$\rho(i, E) = \frac{1}{\pi} \sum_n |\psi_n(i)|^2 \mathrm{Im} \frac{1}{E - E_n + i\varepsilon}. \tag{4.1}$$

We applied a small broadening $\varepsilon \approx 20$ meV of levels into a Lorentzian shape, which is both expected to exist in the material and leads to smoothing of the finite size effects in the LDOS . We introduce the defects by inserting a line of extra atoms, thereby creating a defect—anti-defect pair at a maximum separation of half the graphene patch size. By adding an additional line of atoms, we can study the LDOS of two defect cores close to each other, isolated from their anti-defects. The Hamiltonian is of the single particle spin degenerate tight-binding graphene:

$$H = - \sum_{<ij>} t_{ij} (c_i^\dagger c_j + H.c.), \tag{4.2}$$

with the hopping constant $t = 2.7$ eV. When choosing the nearest neighbor pairs in Eq. (4.2), we retain the topology of the honeycomb lattice, which is violated only at a single atom in the "OCT" dislocation case. The LDOS turns out to be robust to relaxation of bond lengths, so that the results for $t_{ij} = t$ are representative.

Our calculation shows that the LDOS at the dislocation cores is insensitive to the distance between the dislocations, in particular the LDOS peak at zero energy in the "OCT" type core system stays pinned and does not hybridize when the defects are brought close to each other to minimal distance of few lattice constants.

The results of the tight-binding model presented in this section show that the characteristic features of the dislocation LDOS , notably the zero energy peak of the "OCT" core fall-off with distance from the core as a power law (Fig. 4.1). This is the expected behavior according to low energy continuum models of graphene (see Section 4.2.2), and also argued for in the case of cracks in graphene in Ref. [172].

The STS measurements of Ref. [171], achieving atomic resolution, however show an exponential fall-off of LDOS features with the distance from the prominent defect centers, even for defects far from each other. This discrepancy might

be due to subtle shortcomings of substituting a simplified single graphene sheet for the top layer of graphite; however, another explanation could be the presence of stronger disorder. The fact that the single atom resolution along the grain boundary is lost in patches of several lattice constants across also indicates that the grain boundary might contain more disorder than an array of simple dislocations. This presents additional motivation for our study of amorphous tilt grain boundaries presented in Section 4.3, in place of the coherent ones studied in Refs. [166, 170, 191].

4.2.2 Continuum model of dislocations

It is interesting and fundamental to approach the description of grain boundaries by considering an analytical model. In this Section, we describe the results of such a continuum model, finding conditional agreement with the tight-binding results. We then proceed to use the theory for describing the LDOS of an array of dislocations, and find a surprising prediction of localized modes at zero energy. Even if the continuum theory prediction fails in a more realistic model (as Ref. [170] suggests), we find it a fundamental step in understanding the system.

The continuum description of the topological effect of dislocations on the graphene electrons was introduced in detail in Chapter 2. We however choose to summarize it here, and introduce relevant notation. The defect acts as a translation by the Burgers vector $\vec{b}$ of the wavefunction of the ideal crystal, upon encircling the defect core. The model is therefore an Aharonov-Bohm (AB) effect without breaking time reversal symmetry. We start from the Hamiltonian in the form of the standard graphene Dirac equation, coupled to a dislocation gauge field:

$$H_{disl} = -i\hbar v_F \tau_0 \otimes \vec{\sigma} \cdot (\vec{\nabla} - i\vec{A}), \tag{4.3}$$

where the dislocation gauge field $\vec{A}$ (in fixed gauge) produces the correct pseudoflux of the translation holonomy $\oint \vec{A} \cdot d\boldsymbol{x} \equiv (\boldsymbol{K} \cdot \vec{b})\tau_3 = 2\pi d\ \tau_3$, e.g. $A_\varphi = \frac{(\boldsymbol{K}\cdot\vec{b})}{2\pi r}\tau_3 = \frac{d}{r}\tau_3$, where r and φ are the standard polar coordinates. The Burgers vector is encoded in the dislocation pseudoflux d which has only three inequivalent values $\{0, \frac{1}{3}, -\frac{1}{3}\} \equiv \{0, -\frac{1}{3}, -\frac{2}{3}\}$, opposite at the two Fermi points. We label a Fermi wavevector by $\boldsymbol{K}$ (and the other Fermi point is at $-\boldsymbol{K}$), τ matrices mix the two Dirac points, the σ matrices act on the A/B sublattice, and we use the four component spinor $\Psi(\boldsymbol{r}) \equiv (\Psi_{\boldsymbol{K}_+ A},\ \Psi_{\boldsymbol{K}_+ B},\ \Psi_{\boldsymbol{K}_- B},\ -\Psi_{\boldsymbol{K}_- A})^T$.

An important property of the translation operator, and consequently the $\vec{A}$ gauge field, is that it does not mix the Fermi points, so that we can consider them separately. Therefore our model is based on a single valley Dirac equation in the AB field of flux $d \in \{-\frac{1}{3}, -\frac{2}{3}\}$:

$$H_+^d = -i\hbar v_F \vec{\sigma} \cdot \left(\vec{\nabla} - i\frac{d}{r}\vec{e_\varphi}\right). \tag{4.4}$$

The other valley experiences the complementary flux $-1-d$, i.e. $H_-^d = H_+^{-1-d}$. We have chosen the values of d such to conform to the practice of AB flux being the fractional flux part.

To test this theory, we find the LDOS in patch of radius δ covering the defect:

$$\rho(\delta, E) \sim \delta^{4/3}|E|^{1/3}. \tag{4.5}$$

This agrees with the tight-binding model results in the limit where the bipartiteness of the honeycomb lattice is not broken in the defect, Fig. 4.1(c). This is exactly the limit in which we expect the topology effects in the hopping network to be dominant, and is possible in both core cases. In the "OCT" case the undercoordinated atom as an intruder, but otherwise the bipartitness and topology of the ideal lattice are preserved. In the "PH" core case, the bond which spoils the hopping bipartiteness (nominally an A-A bond, cf. inset of Fig. 4.1(a)) is switched on, it contends with the purely topological effect of the dislocation, and introduces asymmetric features in the LDOS (Fig. 4.1(a)). The precise nature of the asymmetric features is clearly identified by considering the LDOS of an isolated 10 atom ring which is turned into a pentagon—heptagon structure by switching on the A-A bond, Fig. 4.1(b).

We now outline the calculation leading to Eq. (4.5), which is also fundamental for understanding the prediction for a dislocation array. The eigenfunctions of Eq. (4.4) are found by separating the angle, and we find for energy $E = \epsilon\hbar v_F\lambda$ ($\epsilon = \pm 1$ and $\lambda > 0$):

$$\Psi_E^s(\boldsymbol{r}) = \sum_{m\in\mathbb{Z}} e^{im\varphi} \begin{pmatrix} e^{-i\varphi}u_m^s(r) \\ \epsilon i v_m^s(r) \end{pmatrix}, \tag{4.6}$$

where the sign $s \in \{+,-\}$ labels two linearly independent solutions $\psi_m^s \equiv (u_m^s(r), v_m^s(r))^T = (J_{s(m-1-d)}(\lambda r), J_{s(m-d)}(\lambda r))^T$, and J_q is the Bessel function of order q (note that $q \notin \mathbb{Z}$). The total angular momentum in channel m is $j = m - 1/2$, and we see that the presence of dislocation shifts it $j \to j - d$. Normalizability allows exclusively ψ_m^+ for $m > 0$, and ψ_m^- for $m < 0$, and both for $m = 0$. The Hamiltonian Eq. (4.4) is actually not self-adjoint, so that there is additional physical input needed regarding the wavefunction boundary condition at the singular point at the defect. The application of the standard theory of self-adjoint extensions (SAE) [192–195] says that the coefficients of the linear combination $N_+\psi_0^+ + N_-\psi_0^-$ in channel $m = 0$ determine the additional physical parameter $\chi \in [0, 2\pi)$ through

$$N_+/N_- = \cot(\chi/2). \tag{4.7}$$

The channel $m = 0$ actually contains normalized spinors $\psi_m^{+/-}$ which have diverging components on the sublattice A/B respectively, and the ratio of these divergences is set by the particular SAE through the value of χ.

We can now evaluate the LDOS in a patch of radius δ, [112]

$$\rho(\delta, E) = 2\pi \int_0^\delta r dr \sum_{\epsilon,\lambda} \sum_m |\psi_m(\lambda r)|^2 \delta(E - E_\lambda) \sim \tag{4.8}$$

$$\sim \int \lambda d\lambda \int_0^\delta r dr \, (r\lambda)^{2q} \, \delta(E - \hbar v_F \lambda) \sim \tag{4.9}$$

$$\sim \delta^{2q+2} |E|^{2q+1}, \tag{4.10}$$

where in the second line we have used the Bessel function density of states $\sum_\lambda \to \int \lambda d\lambda$, and evaluated the small argument (i.e. $\lambda r \ll 1$) expansion of the Bessel functions of order q. The leading contribution comes from the diverging components of ψ_0, where $q = -1/3, -2/3$ (this holds for both Fermi points, and both dislocation classes).

The value of $q = -2/3$ generates an unphysical divergence $\rho \sim 1/|E|^{1/3}$. We therefore have to choose the SAE which removes the offending part of ψ_0, and this turns out to be $\chi = \pi$ and $\chi = 0$, for $d = -1/3$ and $d = -2/3$, respectively. Note that at the second Fermi point, we have to switch the values, so that $\chi = 0, \pi$ for $d = -1/3, -2/3$. The surviving components in ψ_0 with $q = -1/3$ give the advertised patch LDOS of Eq. (4.5).

4.2.3 Continuum model of dislocation arrays

Once we know the details of the continuum description of a graphene dislocation derived in the previous subsection, we can ask the question what happens in an array of such defects? As we have shown, the SAE of the continuum Hamiltonian of Eq. (4.4) is fixed by the allowed values of $\chi = 0, \pi$. It turns out that precisely these special values of χ allow the Hamiltonian to have localized states at zero energy. This leads to a peak at zero energy which is absent from the gapless, cusp shaped LDOS of the finite energy wavefunctions in Eq. (4.5).

It is well known, that Hamiltonians with singular potentials (e.g. AB flux, [196] Coulomb potential, [194] delta function potential [195]), once they are made Hermitian through a SAE, can exhibit finite or zero energy bound states, even if the original Hamiltonian was scale-free.

Our system is represented by two copies (two Fermi points) of a two-component, two dimensional spinor in the presence of a pseudomagnetic solenoid with flux $d \in \{-1/3, -2/3\}$. The problem of a spinful two dimensional particle moving in an arbitrary magnetic field, both non-relativistic (Pauli) and relativistic (Dirac), has originally been considered by Aharonov and Casher, [197] who found that the number of flux quanta give the number of zero-energy states of the particle. In Ref. [196], the Dirac particle in presence of multiple AB solenoids is considered, so we can here directly use those results concerning the zero modes of the Dirac Hamiltonian of the form Eq. (4.4).

Let us describe the relevant calculation, following Refs. [196,197] closely. The fact that $\chi = 0, \pi$ is the key ingredient: as we have seen in Section 4.2.2, at

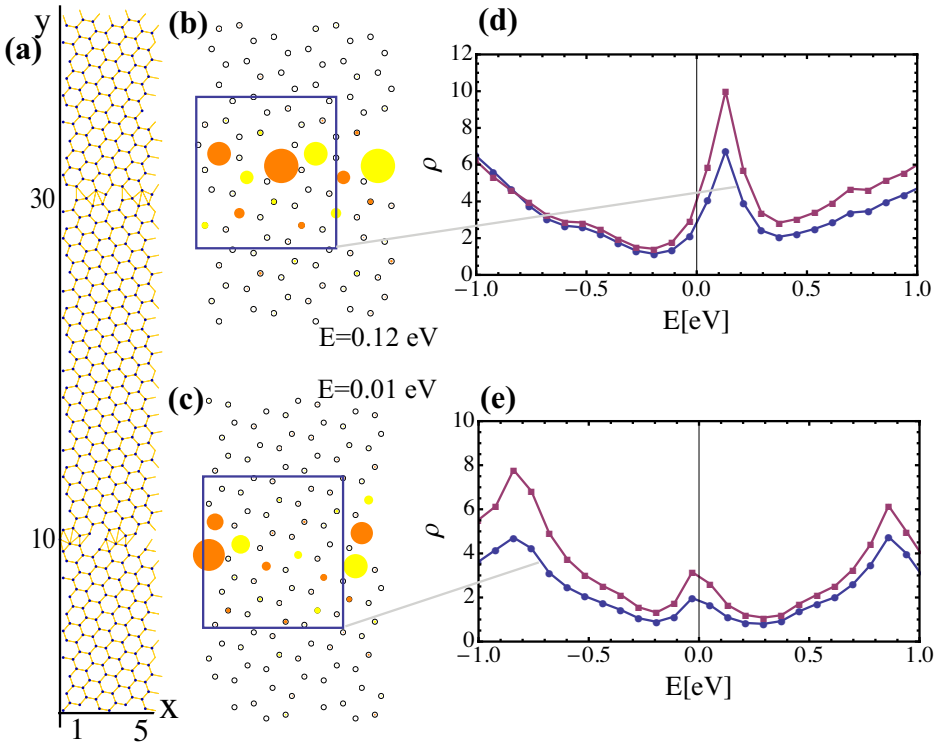

Figure 4.2: The LDOS and states of tight-binding amorphous tilt grain boundary: example of armchair type with medium opening angle. (a) The system with hoppings (of different strength in calculation) included. (b),(c) Zoom-in of the boundaries, including the wavefunctions at $k_x = 0$ at energy of the LDOS peaks: size of colored dots is the amplitude, orange (dark grey) and yellow (light grey) denote opposite sign. (d),(e) The LDOS of two grain boundaries, averaged within square patches as marked in (a).

these values the divergence of the wavefunction is allowed in only one of the spinor components. This means that the SAE imposed boundary condition on the wavefunction does not mix the two components, i.e. sublattices. For zero energy, the eigenproblem of H_d^+ also decouples the sublattices. Going to complex coordinates $z = x + iy$, $A = A_x + iA_y$, and using the scalar potential $\Phi(z) = -\sum_i^n d_i \log|z - z_i|$ of the AB gauge potential of dislocations d_i at positions z_i (i.e. $\partial_z \Phi(z) = A$), we can solve for the two sublattices separately: $\partial_{z^*}(e^{-\Phi}u) = 0$ and $\partial_z(e^{\Phi}v) = 0$. The Dirac equation now tells us that $e^{-\Phi}u$ ($e^{\Phi}v$) is an analytic (antianalytic) function outside the singular points z_i. For $\chi = \pi$, u cannot have singularities according to Eq. (4.7). Taking into account the behavior $e^{-\Phi} \sim |z|^{\phi}$, $|z| \to \infty$, with $\phi = -\sum_i^n d_i$ the total pseudoflux, it follows that u can be a polynomial of z of order at most $\{-\phi\} - 1$, where $\{\}$ is the lower integer part. There are $\{-\phi\}$ linearly independent such polynomials. In the case $\chi = 0$, v is not singular so that $e^{\Phi}v$ vanishes at the defects. v is a polynomial in z^* of degree $\{\phi\} - 1$, with n zeros, and there are $\{\phi - n\}$ of them.

Collecting the results, there are $\{|\phi - n|\}$ ($\{|\phi|\}$) zero modes in the case $\chi = 0$ ($\chi = \pi$) for the single Fermi point system. Note that we assumed the same value of χ for each dislocation d_i, so that the result is only in the case of all dislocations having equivalent Burgers vectors, which is the case of a grain boundary! The two Fermi points contribute independently to the number of zero modes, and since χ and d_i are reversed between them, we get a total of

$$D = \{|2\phi - n|\} + \{|\phi|\}, \text{ with } \phi = \frac{n}{3}, \tag{4.11}$$

zero modes in graphene with an array of n dislocations having the same Burgers vector (of whichever non-trivial class d). This number takes the values $D = 2, 2, 2, 4, 4, 4, 6\ldots$, starting at $n = 4$ and onwards. More precisely, we get $D = 2\{n/3\}$, so that D scales with the system size, i.e. $D \sim \frac{2}{3}n$ in the thermodynamic limit.

The zero energy modes are localized at the defects and have a power-law shape. To answer the question of whether they are observable, we look at how the LDOS in a patch of radius δ scales in comparison to the LDOS contribution of the finite energy states Eq. (4.5). Near the defect at z_i, at one Fermi point the u spinor component (sublattice A) scales as $|z - z_i|^{-d}(z - z_i)^p$, where $p \leq \{-\phi\} - 1$ and the value of d is $-1/3$. This gives a contribution $\rho(\delta) \sim \delta^{2p-2d+2}$. The same sublattice at the other Fermi point contributes through $v \sim |z - z_i|^{1+d}(z - z_i)^t$, with $t \leq \{n - \phi\} - 1$, giving $\rho(\delta) \sim \delta^{2t-2d}$. In the case of the opposite defect type, we get the same scaling, but on sublattice B. The leading contribution in the LDOS comes from the minimal values of $p = 0$ and $t = 0$, giving one mode at the defect with the LDOS

$$\rho^{(0)}(\delta) \sim \delta^{2/3}. \tag{4.12}$$

The scaling shows that the zero mode contribution $\rho^{(0)}$ is more favourable than

the finite energy contribution $\rho(\delta, E) \sim \delta^{4/3} E^{1/3}$ at smaller δ, because the strongest zero modes are more localized than all the finite energy wavefunctions.

Since in this Section we dealt with a Dirac particle, it is interesting to consider the number of zero modes through the Atiyah—Singer theorem: In graphene with disclinations this was done in Ref. [198] by using the defect gauge field of a disclination. There it was shown that the number of zero modes is proportional to the Euler characteristic of the manifold. The key to the application of the theorem is that graphene with disclinations can form compact manifolds, e.g. the fullerene molecule, so that the mapping of the lattice and hopping topology onto a compact continuum manifold is correct, leaving the low energy Dirac particle description valid. For the case of dislocations however there is no such possibility. The exception is the map from the dislocated lattice onto the torus (i.e. the plane with periodic boundary conditions), but this is possible only when for every dislocation there is an anti-dislocation. In that case, the theorem predicts no zero modes, in accordance with our present calculation.

4.3 Tight-binding model of relaxed amorphous grain boundaries

4.3.1 The method

We consider two misoriented graphene grains of same width, confined in a periodic box of width L_y and length L_x. The nominal box boundaries at $y = 0, L_y$ are positioned through the middle of the width of the "first" grain. The second grain is generated in the middle half of the box (from $L_y/4$ and $3L_y/4$) and both grains are periodic with the box in the x direction. The boundaries at $x = 0$ and $x = L_x$ have twisted PBC so that the system is a periodic crystal of length $N * L_x$ (we set $N = 18$), with momenta $k_x = 2\pi/(NL_x)$. The lattice of each grain is generated from its center, and terminated at the grain boundaries. The boundaries are symmetric, but in general the two grain boundaries do not have the same structure because the two grains have different centers of inversion symmetry.

The allowed values for the grain's orientation θ_i follow from the constraint of its periodicity with the box along the x direction. If $\vec{L}' = a_i\vec{e}_1 + b_i\vec{e}_2$ is the vector in the basis of the graphene Bravais lattice which is to be wrapped along the x box direction, the constraint is

$$\cos(\theta_i) = \frac{a_i + b_i/2}{a_i^2 + b_i^2 + a_i b_i/2},$$

as also explicated in Ref. [199]. If we allow slight strain in the grain, the number of available orientations can be enlarged. [199] The grain opening angle $\theta = \theta_1 - \theta_2 = 2\theta_1$ spans the entire $[0°, 30°]$ range (for both zigzag and armchair type [170, 171]).

We relax the atoms in the system at zero temperature using the molecular dynamics method, where the interatomic potential for carbon is taken in the Tersoff—Brenner form. [200, 201] The potential between atoms i, j at distance r_{ij} is

$$\begin{aligned} V(r_{ij}) &= V_R(r_{ij}) - \bar{B}_{ij} V_A(r_{ij}) \\ V_R(r) &= \frac{D}{S-1} e^{-\sqrt{2S}\beta(r-R)} f(r) \\ V_A(r) &= \frac{DS}{S-1} e^{-\sqrt{2/S}\beta(r-R)} f(r), \end{aligned}$$

with $f(r)$ the smoothing function

$$f(r) = \begin{cases} 1, & r < R_1 \\ \frac{1}{2}\left(1 + \cos\left[\frac{(r-R_1)\pi}{R_2-R_1}\right]\right), & R_1 < r < R_2 \\ 0, & r > R_2. \end{cases}$$

The effect of bond angles is encoded in $\bar{B}_{ij} = 1/2(B_{ij} + B_{ji})$, with

$$B_{ij} = \left(1 + \sum_{k \neq i,j} G(\theta_{ijk}) f(r_{ik})\right)^{-\delta},$$

where θ_{ijk} is the angle between the $i-j$ and $i-k$ bonds, and the function G is

$$G(\theta) = a_0 \left(1 + \frac{c_0^2}{d_0^2} - \frac{c_0^2}{d_)^2 + (1 + \cos(\theta))^2}\right).$$

The ground state of this non-spherically symmetric potential is the graphene honeycomb lattice, when the parameters are chosen as in Ref. [201]: $D = 6$ eV, $R = 0.139$ nm, $\beta = 21\ nm^{-1}$, $S = 1.22$, $\delta = 0.5$, $a_0 = 0.00020813$, $c_0 = 330$, and $d_0 = 3.5$. The smoothing cutoffs are chosen to include the nearest neighbor atoms, $R_1 = 0.17\ nm$ and $R_2 = 0.2\ nm$.

When the lattice is formed, we consider a tight-binding model for electrons, of the form Eq. (4.2). The hopping constants t_{ij} are taken to fall-off exponentially, and fitted so that t_{ij} for the nearest neighbor distance $|\Delta|$ is $t = 2.7$ eV, and for the next-nearest neighbor distance $\sqrt{3}|\Delta|$ it is $t' = 0.1$ eV, in accordance with accepted values for graphene. [202] Finally, we extract the energy bands $E(k_x)$, the wavefunctions $\psi_E(i)$ and the LDOS $\rho(i, E)$.

4.3.2 Summary of results

We analyze in detail a number of grain boundaries of both zigzag and armchair type, [170, 171] covering the entire range of opening angles by varying the box size: $2.6a < L_x < 16.1a$ with $a = 0.246$ nm the graphene Bravais lattice constant.

In summary, we find that the LDOS along the grain boundaries, averaged in square patches of size $4a$ and considered in the low energy regime of $|E| < 1$ eV, shows three typical behaviors:

(i) A peak at very small energy, $|E| < 0.05$ eV

(ii) Two peaks at nearly opposite energies, at around $0.3 \text{ eV} < |E| < 0.5$ eV

(iii) Just one peak, at an energy $0.3 \text{ eV} < |E| < 0.5$ eV.

Focusing on case (i), we have determined that the lowest energy wavefunctions are sometimes localized on structures that resemble short zigzag edge segments (i.e. of length $2a$). This however occurs also in armchair type boundaries, but of course then the short zigzag segment is tilted away from the grain boundary line, the x axis. In some systems however, the zero energy peak is associated with overcoordinated atoms, having even five neighbours.

We find that clear examples of case (ii) mostly appear at high opening angles (i.e. small L_x), where the strong LDOS signal spans the entire grain boundary. There are also just a few energy bands with $|E| < 1$ eV, so it is easy to identify that the LDOS peaks are due to van Hove singularities, in accordance with the findings of Ref. [170] for large opening angles.

The case (iii) we find is strongly correlated with carbon atoms that were annealed into a position with four neighbors, meaning that four atoms are within the $|\mathbf{\Delta}|$ distance, distributed roughly evenly around the central atom.

Since the LDOS behavior of case (ii) has already been identified in Ref. [170], we illustrate the occurrence of cases (i) and (iii) through typical examples Figs. 4.2,4.3,4.4.

Finally, we note that typically there is one localized region within the box that has atoms with high LDOS values, i.e. one can say that there is one prominent "defect" within one L_x long unit-cell of the entire grain boundary. This means that the periodicity of grain boundary calculated from the opening angle corresponds to the periodicity of prominent defect structures, even in our case of amorphous boundaries. [171] There are rare special cases where our box has an accidental symmetry so that the defect structures along the boundary repeat twice within the box length L_x, effectively halving L_x and θ.

4.4 Discussion and conclusions

We have analyzed the problem of dislocation models of graphene (graphite) grain boundaries, and analyzed a model of an amorphous grain boundary. We find that by taking into account the possible stable structures of the simplest dislocations (Burgers vector equal to lattice constant), one can expect both zero energy and finite energy peaks in the LDOS , as observed in STS measurements. Within a continuum description of dislocated graphene in the form of a gauged Dirac equation, we find that in fact arrays of dislocations (which comprise grain

boundaries) can lead to zero energy states, without any undercoordinated atoms at their core. In view of clues that the grain boundaries might be disordered beyond the simple dislocation array, we have introduced a tight-binding model of relaxed amorphous grain boundaries. We find that the variety of structures that stabilize at the boundary lead to narrow bands both close and away from zero energy.

The natural next step is to inspect the magnetic properties of the amorphous grain boundaries, when the interaction between electrons is switched on. Due to the LDOS enhancement, we expect magnetic moments along the grain boundary, to be compared to the results of AFM scans of graphite in Ref. [171]. This might provide a concrete model for (existence of) ferromagnetism found in extended defects on the graphite surface.

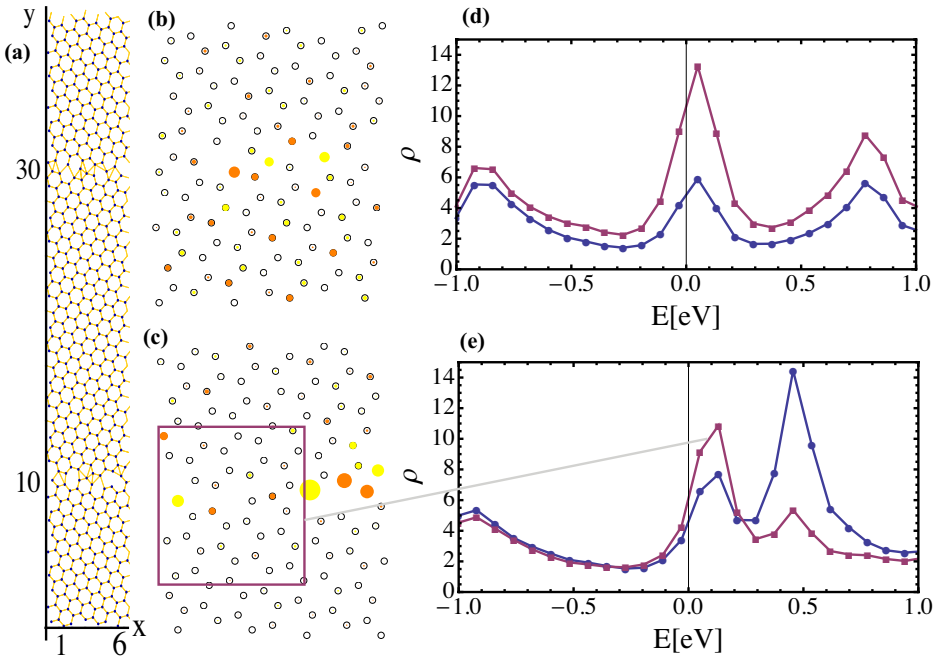

Figure 4.3: The LDOS and states of tight-binding amorphous tilt grain boundary: example of zigzag type of medium opening angle. (a) The system with hoppings (of different strength in calculation) included. (b),(c) Zoom-in of the boundaries, including the wavefunction at $k_x = 0$ and $E = 012$ eV: size of colored dots is the amplitude, orange (dark grey) and yellow (light grey) denote opposite sign. (d),(e) The LDOS of two grain boundaries, averaged within square patches as marked in (a).

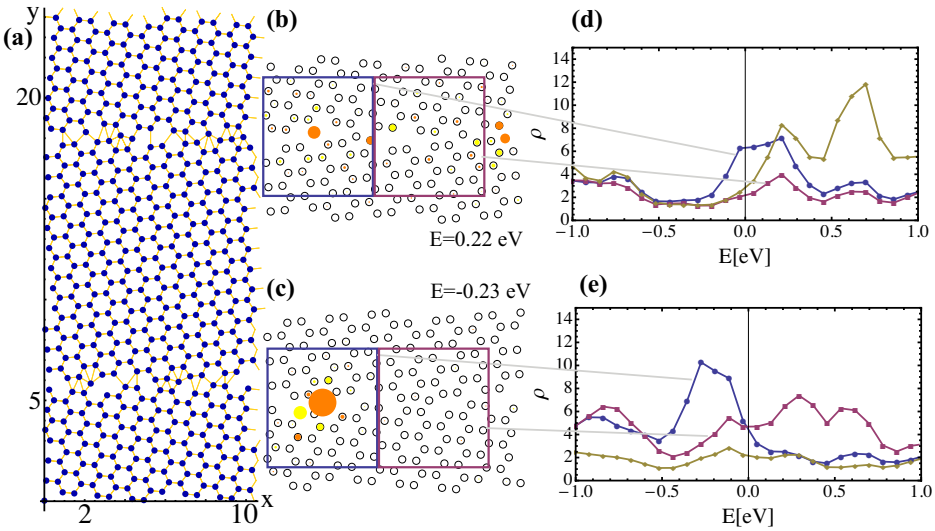

Figure 4.4: The LDOS and states of tight-binding amorphous tilt grain boundary: example of armchair type of small opening angle. (a) The system with hoppings (of different strength in calculation) included. (b),(c) Zoom-in of the boundaries, including the wavefunctions at $k_x = 0$ at E of the peaks: size of colored dots is the amplitude, orange (dark grey) and yellow (light grey) denote opposite sign. (d),(e) The LDOS of two grain boundaries, averaged within square patches as marked in (a).